"Flow Modelling and Turbulence Measurements VI", pp. 407-414, Eds. C.-J. Chen, C. Shih, J. Lineau and R.J. King.

Reynolds Stress modeling of complex flows over curved surfaces

Sven Perzon Lars Davidson
Dept. Thermo- and Fluid Dynamics
Chalmers University of Technology
S-412 96 Göteborg, Sweden

Mats Ramnefors
Volvo Data AB
S-405 08 Göteborg, Sweden

Abstract

Curved three dimensional boundary layers are regarded using Second moment closures. Different models have been tested on one internal and one external flow case. The results are more accurate using a Reynolds stress model compared to an eddy viscosity model, e.g. the k-ε-model. Even so, the k-ε-model predicts the pressure distribution, on the prolate spheroid test-case, more accurate than any of the Reynolds stress models tested.

Furthermore it is shown that it is worth while to use a realizable pressure strain model that need no wall reflection terms in terms of both accuracy and stability. It is a fact that a CFD-code of any generality usage have to use this type of model to succeed with a Reynolds stress model.

1. Introduction

Computational fluid dynamics, CFD, have not yet been fully accepted as the engineering tool in aerodynamic design processes. CFD is not regarded as trustworthy enough for this purpose. Thus aerodynamic design processes still heavily depend upon experiments. However industrial and commercial CFD softwares are being used more and more, but many of these have only simple turbulence models available such as models based on the eddy viscosity assumption. Thus the eddy viscosity models are often used in industry even though they are known to erroneously mimic the behaviour of the turbulence in complex flow situations such as curved flows including separation. However many results obtained using eddy viscosity models, EVMs, are surprisingly accurate, see Ramnefors *et al.* [3].

Second-moment closures have been used as an alternate and more physical approach to the problem. Computer have now become fast enough to allow these Reynolds stress models, RSMs, to be used in full three dimensional simulations. RSMs are however not used very frequently for engineering purposes because of problems with how to cope with walls in a general manner and lack of numerical robustness which is not built in naturally into the model in the same fashion as what is done in EVMs.

RSMs are, just as EVMs, usually designed for simple two dimensional test cases. Industrial needs are numerically robust codes including turbulence models that are

capable of describing the proper turbulent structures in very advanced three dimensional flow situations. Even if a RSM is used this is not a priori known to be true, see Schwarz & Bradshaw [13]. Expectations are however that RSMs should be more accurate than EVMs in complex three dimensional flows because of its exact approach for the source terms that physically maintains the turbulence.

In this work, several RSMs are tested on two test-cases. One test-case is the flow through a bent rectangular channel and comparisons are made towards experiments by Kim & Patel [7]. The other test-case is the flow over a prolate 6 to 1 spheroid at a 10 degrees angle of attack. Comparisons are made towards several experiments by Ahn [2], Chesnakas & Simpson [4] and Kreplin & Stäger [8]. Both test-cases are three dimensional and quite complex in character why they are delicate tasks for any turbulence model.

The commercial flow solver CFX4 [1] is used. In order to be able to implement new turbulence models we have access to relevant parts of the source code.

2. Turbulence models

The model equation for the Reynolds stresses $\overline{u_i u_j}$ in an incompressible flow using the generalized gradient diffusion hypothesis GGDH [5] for the turbulent diffusion becomes,

$$\frac{D\overline{u_i u_j}}{Dt} = -\left(\overline{u_i u_k}\frac{\partial U_j}{\partial x_k} + \overline{u_j u_k}\frac{\partial U_i}{\partial x_k}\right) + \phi_{ij} - \varepsilon_{ij} + \frac{\partial}{\partial x_k}\left(c_s \overline{u_l u_k}\frac{k}{\varepsilon}\frac{\partial \overline{u_i u_j}}{\partial x_l} + \nu\frac{\partial \overline{u_i u_j}}{\partial x_k}\right) \quad (1)$$

Most models differ mainly in the modeling of the pressure strain interaction term ϕ_{ij}. A model exists already in CFX4 and it is the return to isotropy term by Rotta [12] combined with the Isotropization of Production term by Naot *et al.*[11](IP).

$$\phi_{ij} = c_1 \varepsilon a_{ij} + c_2\left(P_{ij} - \frac{2}{3}P_k \delta_i j\right) \quad (2)$$

where $a_{ij} = \overline{u_i u_j}/k - 2/3\delta_{ij}$ is the anisotropy tensor. This model has no wall correction terms and mimics the stress distribution erroneously if a wall is present.

The wall reflection model of Gibson and Launder [6], (GL), has been added to the IP-model in this work and is used in a form that takes only the closest wall into account. In addition to these models a nonlinear cubic proposal by Launder and Li [9] (LLI) has been tested. One of the benefits gained from the latter model is the fact that it seem to work fairly well without wall reflection terms.

The dissipation term is modeled using the assumption that the small scales are locally isotropic, $\varepsilon_{ij} = 2/3\varepsilon\delta_{ij}$.

Wall-functions are used at the wall boundaries and the stresses are handled according to the proposal of Lien and Leschziner [10] extended to three dimensions. Dissipation rate is set as, $\varepsilon = U_*^3/(\kappa\eta_{\text{wall}})$, at the node adjacent to the wall. Furthermore the stresses are set in a local stream aligned coordinate system with unit base vectors $\vec{t} = (t_x, t_y, t_z)$ and $\vec{n} = (n_x, n_y, n_z)$. $\vec{n}$ is the unit wall normal vector and $\vec{t}$ is the unit wall tangential vector that is aligned with the flow. The third component in this orthogonal set of base vectors is taken as the cross-product of $\vec{t}$ and $\vec{n}$. The stresses in this locally symmetric flow are set as $(\overline{uu})' = 1.098k$, $(\overline{vv})' = 0.247k$ and $(\overline{uv})' = -0.255k$ where $k = U_*^2/\sqrt{c_\mu}$. Note that due to symmetry, $(\overline{vw})' = (\overline{wu})' = 0$. U_* is computed from the log law. A simple coordinate

transformation will then render the following stresses at the node adjacent to the wall,

$$
\begin{aligned}
\overline{uu} &= t_x{}^2(\overline{uu})' + n_x{}^2(\overline{vv})' + 2\,t_x\,n_x\,(\overline{uv})' \\
&\quad +(\overline{ww})'\,t_y{}^2 n_z{}^2 - 2\,(\overline{ww})'\,t_y\,n_z\,t_z\,n_y + (\overline{ww})'\,t_z{}^2 n_y{}^2 \\
\overline{vv} &= t_y{}^2(\overline{uu})' + n_y{}^2(\overline{vv})' + 2\,t_y\,n_y\,(\overline{uv})' \\
&\quad +(\overline{ww})'\,t_z{}^2 n_x{}^2 - 2\,(\overline{ww})'\,t_z\,n_x\,t_x\,n_z + (\overline{ww})'\,t_x{}^2 n_z{}^2 \\
\overline{ww} &= t_z{}^2(\overline{uu})' + n_z{}^2(\overline{vv})' + 2\,t_z\,n_z\,(\overline{uv})' \\
&\quad +(\overline{ww})'\,t_x{}^2 n_y{}^2 - 2\,(\overline{ww})'\,t_x\,n_y\,t_y\,n_x + (\overline{ww})'\,t_y{}^2 n_x{}^2 \\
\overline{uv} &= t_y\,t_x\,(\overline{uu})' + t_y\,n_x\,(\overline{uv})' + n_y\,t_x\,(\overline{uv})' + n_y\,n_x\,(\overline{vv})' \\
&\quad +(\overline{ww})'\,t_y\,n_z\,t_z\,n_x - (\overline{ww})'\,t_y\,n_z{}^2 t_x - (\overline{ww})'\,t_z{}^2 n_y\,n_x \\
&\quad +(\overline{ww})'\,t_z\,n_y\,t_x\,n_z \\
\overline{vw} &= t_z\,t_y\,(\overline{uu})' + t_z\,n_y\,(\overline{uv})' + n_z\,t_y\,(\overline{uv})' + n_z\,n_y\,(\overline{vv})' \\
&\quad +(\overline{ww})'\,t_z\,n_x\,t_x\,n_y - (\overline{ww})'\,t_z\,n_x{}^2 t_y - (\overline{ww})'\,t_x{}^2 n_z\,n_y \\
&\quad +(\overline{ww})'\,t_x\,n_z\,t_y\,n_x \\
\overline{wu} &= t_z\,t_x\,(\overline{uu})' + t_z\,n_x\,(\overline{uv})' + n_z\,t_x\,(\overline{uv})' + n_z\,n_x\,(\overline{vv})' \\
&\quad +(\overline{ww})'\,t_y\,n_z\,t_x\,n_y - (\overline{ww})'\,t_y{}^2 n_z\,n_x - (\overline{ww})'\,t_z\,n_y{}^2 t_x \\
&\quad +(\overline{ww})'\,t_z\,n_y\,t_y\,n_x
\end{aligned}
$$

The transformations mentioned above was performed using the symbolical mathematical software Maple V. The Fortran source code was produced by Maple V and then incorporated into CFX4. The LLI pressure strain model was coded using a similar technique.

3. Developing flow in curved rectangular duct

The computational domain is shown in figure 1. Inlet profiles are set according to experiments by Kim and Patel [7]. No separation is present but the turbulence is affected by the bend and thus the structure of the secondary motion will change. Experiments are available at several planes along the bend. Comparisons are made with experiments at a plane 45^{o} into the bend which is halfway through the bend.

The mesh contained 194560 cells see figure 1 and was tested for grid independence using a somewhat finer mesh and no difference was discovered.

4. Prolate ellipsoid at incidence

The flow around a 6 to 1 prolate spheroid at incidence has been considered and it is one of the best test-cases available where a three dimensional separation occurs at a curved boundary. The flow pattern is very complex and it is a delicate task for turbulence models trying to mimic the turbulent structures that is present. It is experimentally documented by several authors and present computations are compared to experiments by Chesnakas and Simpson [4], Ahn [2] and Kreplin & Stäger [8]. The computational domain and mesh are shown in figure 5 and the Reynolds number based on the free-stream velocity and the length of the model is $Re_L = 4.2{\cdot}10^6$. The mesh is a 3-block o-type mesh embedded in two blocks upstream and downstream respectively. The number of cells is 326 000. Grid independence has been checked using a somewhat finer mesh and no major difference could be detected.

5. Results

This study contains two test-cases that are very different in character. In the duct flow no separation is present but the secondary motion is affected by the bend and thus the turbulent structure as well. All models do capture the development fairly well, see figures 2 and 3. It is interesting to see the difference between the GL- and the LLI-model since no wall-topography terms is involved in the LLI-model. Still it does capture the development of the flow. The ability of the RSMs to capture the turbulent structures are also remarkable, see figure 4. The LLI-model is best overall and the k-ε-model is the least accurate model.

In the flow over a 6 to 1 prolate spheroid a three dimensional separation is present and the flow structures are very complex. Friction stream traces are shown in figure 6. Comparisons are made to experiments by Kreplin & Stäger [8] where the Reynolds number is larger, that is $Re_L = 7.7 \cdot 10^6$. All models separates too late in comparison with experiments except for the LLI-model. Pressure distributions at walls are available from Ahns [2] experiments and comparisons with simulations are shown in figure 7.

Velocity profiles compared by the experiments of Chesnakas & Simpson are shown in figure 8 and are extracted at $x/L = 0.7622$ in the radial direction of an angle $\beta = 125^{\text{o}}$ from the wind-ward center radius. In the experiments separation at this x location occurs at approximately, $\beta_{\text{sep}} = 123^{\text{o}}$. For the U velocity, the cubic LLI-model matches experiments best at least in shape. The k-ε-model also give fairly accurate results for U. For the vertical and spanwise velocity components all models fails in predicting the proper level. However the shape is more or less correct for all models.

6. Concluding remarks

The standard model in CFX4, that is the IP-model, is very hazardous to use in any wall bounded flow which is shown in figure 8. The GL wall reflections do improve the IP-model however the model behaves somewhat less stable than the IP-model. Best overall is the realizable cubic LLI-model which still proves to be inaccurate in the difficult prolate spheroid case, see figure 8. The LLI-model underpredicts the Reynolds stresses, see figure 4, however gradients of stresses are fairly correct using this model and thus the momentum equations are not affected very much from this fact.

References

[1] AEA Technology, Harwell Laboratory, UK. *CFDS-FLOW3D 3.3 User Guide*, 1994.

[2] S. AHN. *An experimental study of flow over a 6 to 1 prolate spheroid at incidence.* PhD thesis, Virginia Polytechnic Institute and State Univ., Blacksburg, Virginia, 1992.

[3] M. RAMNEFORS, E. HOLMBERG , R. BENDSRYD and S. PERZON. Accuracy of drag predictions on cars using CFD- Effect of grid refinement and turbulence models. In *SAE International Congress & Exposition*, Detroit, USA, 1996.

[4] C.J. CHESNAKAS and R.L. SIMPSON. Full three-dimensional measurements of the cross-flow separation region of a 6:1 prolate spheroid. *Experiments in Fluids*, 17:68–74, 1994.

[5] B.J. DALY and F.H. HARLOW. Transport equation in turbulence. *Phys. Fluids*, 13:2634–2649, 1970.

[6] M.M. GIBSON and B.E. LAUNDER. Ground effects on pressure fluctuations in the atmospheric boundary layer. *J. Fluid Mech.*, 86:491–511, 1978.

[7] W.J. KIM and V.C. PATEL. Origin and decay of longitudinal vortices in developing flow in a curved rectangular duct. *J. Fluids Eng.*, 116:45, 1994.

[8] H.-P. KREPLIN and R. STÄGER. Measurements of the reynolds-stress tensor in the three-dimensional turbulent boundary layer. In *NINTH SYMPOSIUM ON "Turbulent shear flows"*, Kyoto, Japan, 1993.

[9] B.E. LAUNDER and S.-P. LI. On the elimination of wall-topography parameters from second-moment closure. *Phys. Fluids*, 6(2):999–1006, 1994.

[10] F.S. LIEN and M.A. LESCHZINER. Second-moment modelling of recirculating flow with a non-orthogonal collocated finite volume algorithm. In *8th Symp. Turbulent Shear Flows*, Technical University of Munich, Germany, September 1991.

[11] D. NAOT, A. SHAVIT, and M. WOLFSHTEIN. Interactions between components of the turbulent velocity correlation tensor. *Israel J. Techn.*, 8:259, 1970.

[12] J.C. ROTTA. Statistische theorie nichthomogener turbulenz. *Zeitschrift für Physik*, 129:547–572, 1951.

[13] W.R. SCHWARZ and P. BRADSHAW. Turbulence structural changes for a three-dimensional turbulent boundary layer in a 30° bend. *J. Fluid Mech.*, 272:183–209, 1994.

Figures

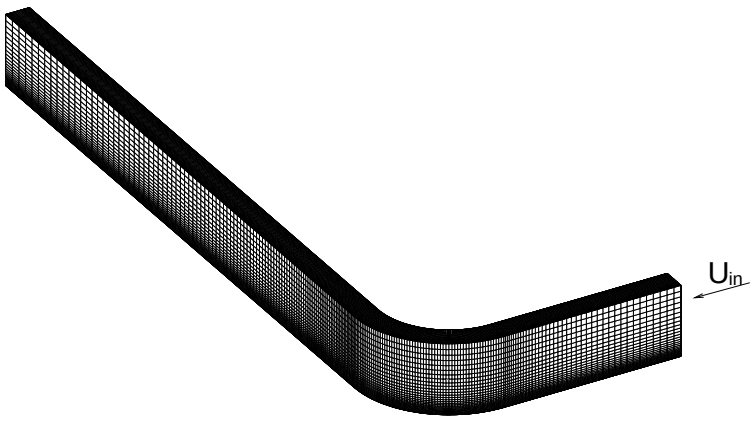

Figure 1: *Domain and grid of the bent rectangular duct.*

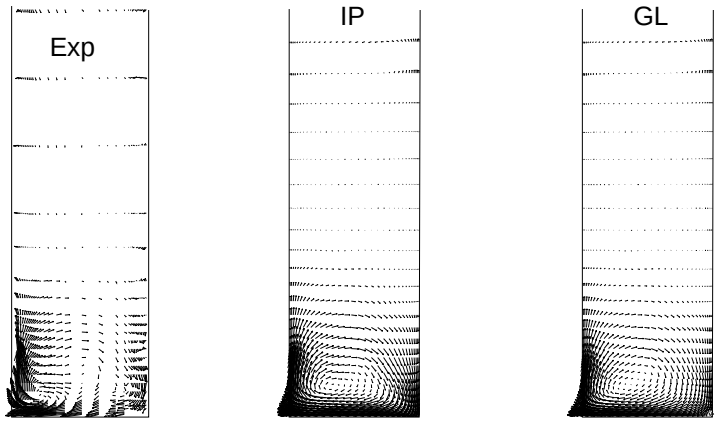

Figure 2: *Secondary velocity field at* 45^o *of the bend.*

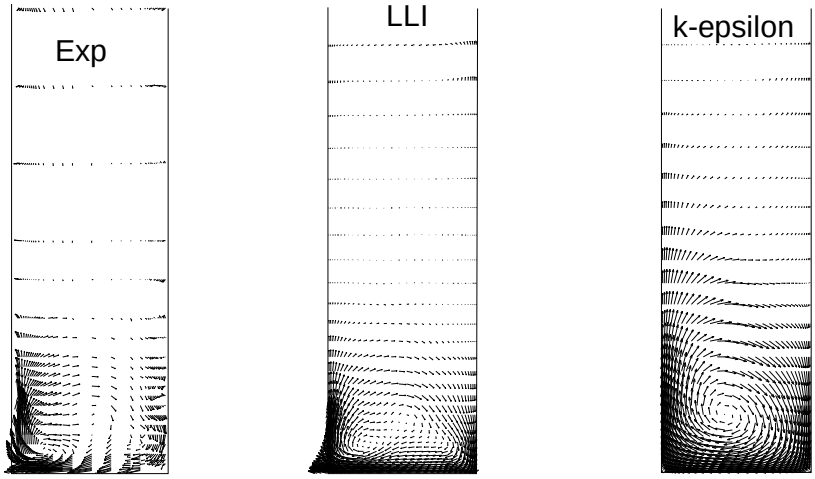

Figure 3: *Secondary velocity field at* 45^o *of the bend.*

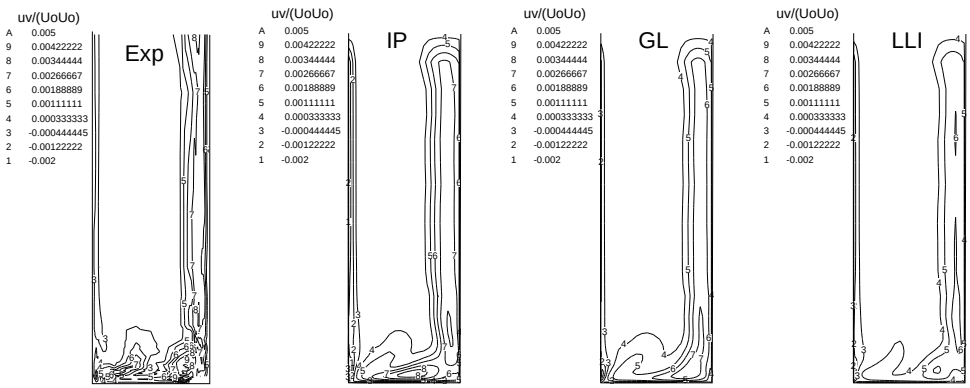

Figure 4: *Shear stress,* $\overline{uv}$*, iso contours at* 45^o *of the bend.*

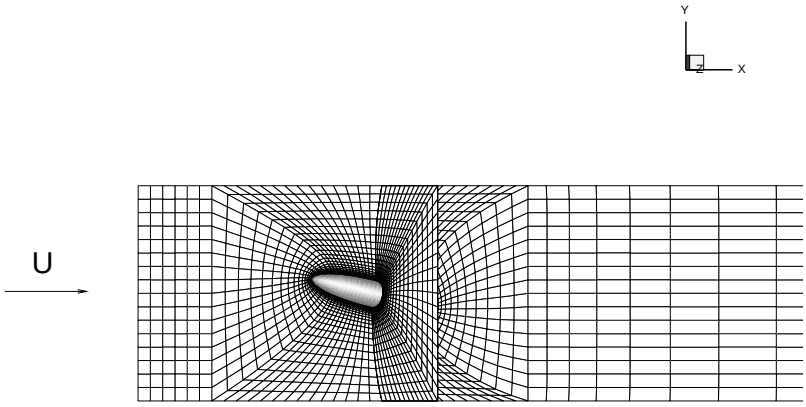

Figure 5: *Domain and grid of the 6 to 1 prolate spheroid. The angle of attack is 10 degrees.*

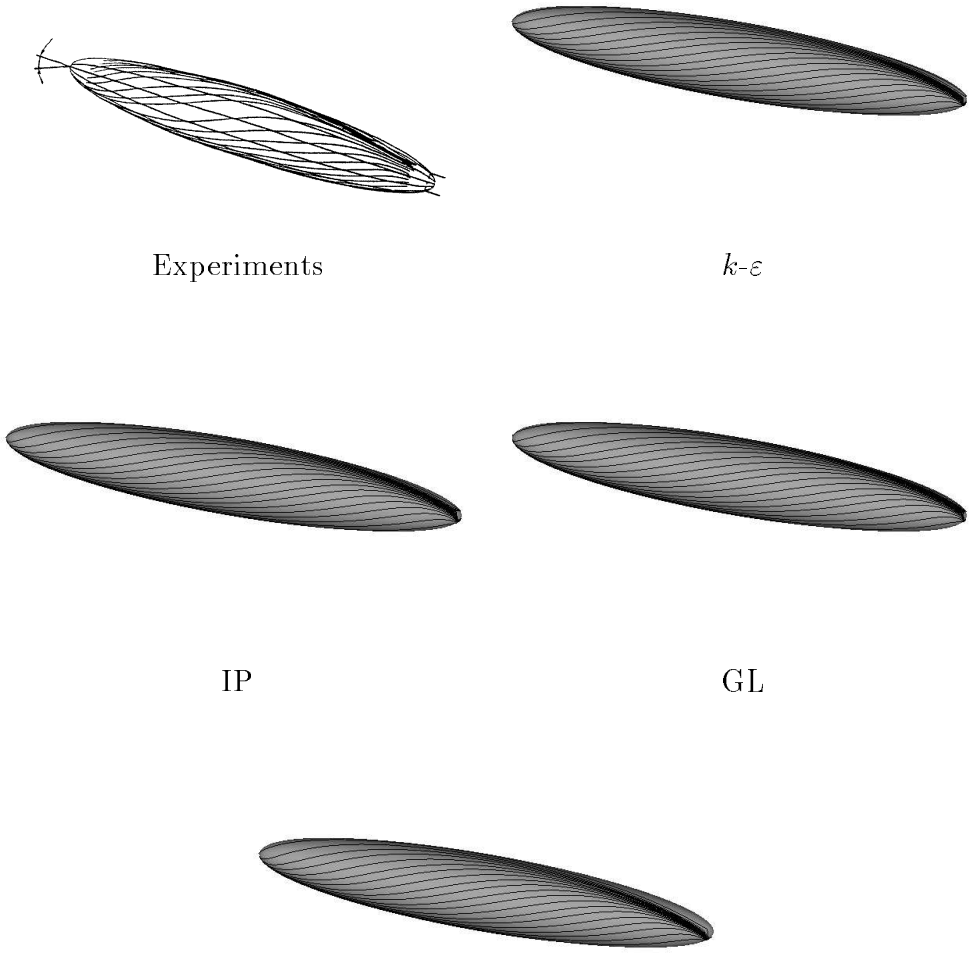

Figure 6: *Friction streamtraces on the surface of the body.*

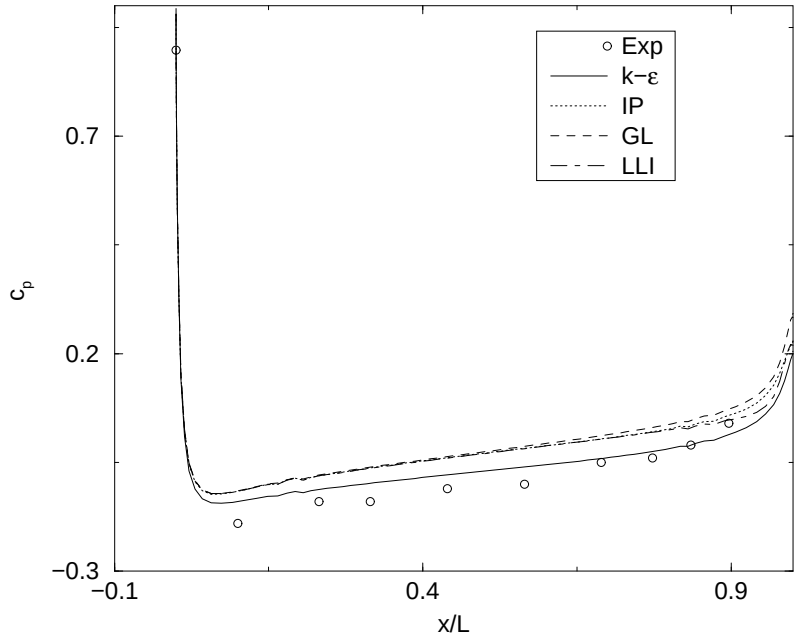

Figure 7: *Pressure coefficient at the wall along the symmetry plane on the suction side.*

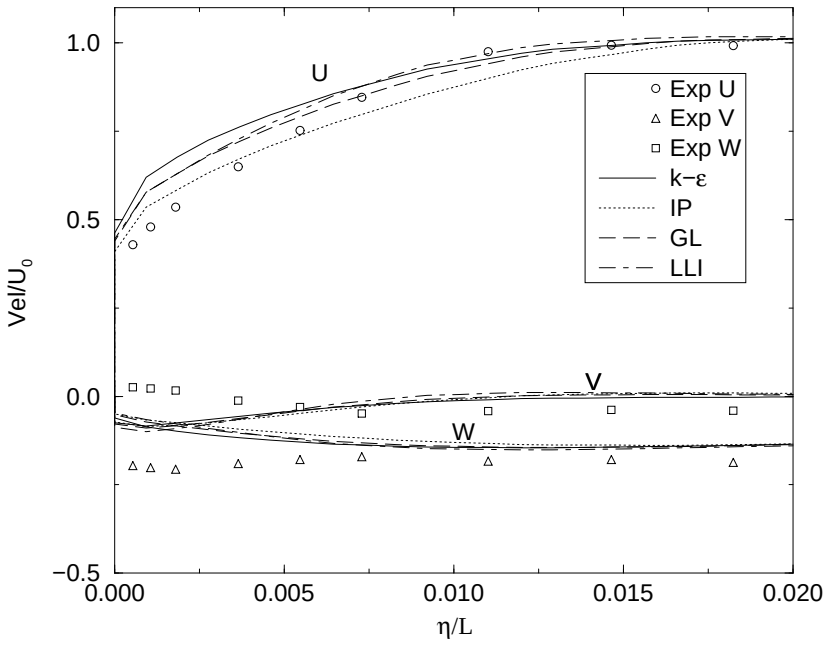

Figure 8: *Velocity at x/L=0.7622 as a function of radial distance from the wall, η. The profile is taken at an angle $\beta = 125^o$ from the center wind-ward side radius.*